Research Article Vol. 30, No. 18 / 29 Aug 2022 / Optics Express 32783
Optics EXPRESS

Experimental demonstration of dispersion-diversity multicore fiber optical beamforming

MARIO UREÑA,* SERGI GARCÍA, JOSE I. HERRANZ, AND IVANA GASULLA

ITEAM Research Institute, Universitat Politècnica de València, Camino de Vera 46022 Valencia, Spain
maurgis@iteam.upv.es

Abstract: Phased array antenna (PAA) beam-steering in high radiofrequency bands will be key for upcoming 5G & Beyond wireless communications systems. As a compact and efficient solution to provide tunable beam steering simultaneously to parallel antenna distribution and connectivity, we experimentally demonstrate, for the first time to our knowledge, tunable optical beamforming implemented on a dispersion-diversity multicore optical fiber. The uniqueness of this fiber lies in the fact that each one of its seven step-index trench-assisted cores has been tailored to provide the required chromatic dispersion to enable tunable optical true-time delay line operation. Continuous 1D beam-steering was demonstrated by measuring the radiating pattern of an in-house fabricated 8-element PAA in an anechoic chamber at the radiofrequency of 26 GHz, sweeping the beam-pointing angle from -43° up to 40° by varying the operating optical wavelength from 1542.50 up to 1548.28 nm. Next-generation fiber-wireless communications systems will benefit from the demonstrated dispersion-diversity MCF optical beamforming in terms of flexibility, versatility, capacity, and connectivity along with reduced size, weight, and power consumption.

1. Introduction

Optical beamforming for phased array antennas (PAAs) will play an essential role in next-generation fiber-wireless communications, especially in very crowded scenarios that require fast and accurate radio beam steering. As its basic building block, the true time delay line (TTDL) is the key optical component that holds high-performance optical beamforming as it prevents undesired beam-squint effects, which can be particularly detrimental in case of broadband signals [1]. Different technologies have been proposed for the implementation of optical TTDL beamforming, including fiber-based architectures that comprise dispersive fibers [2,3], fiber Bragg gratings [4] or parallel single-mode fibers [5], as well as photonic integrated solutions [6]. But despite the intense research activity, there is still need for a compact and efficient fiber-based solution to support antenna radio beam steering along with parallel distribution and connectivity. These properties are of special interest in centralized radio access networks for 5G and Beyond, since they call for multiple-element PAAs with reduced size as they must operate at high radiofrequencies such as the 26-GHz band [7].

Multicore fibers (MCFs) have become one of the leading technologies to overcome the ever-increasing capacity and parallelization demands in fiber-optic communication networks [8]. Beyond high-capacity digital communications, MCFs exhibit great potential in other application scenarios such as radio-over-fiber distribution and MIMO antenna connectivity on one hand, as well as optical and microwave signal processing on the other. In this context, we have previously proposed the use of dispersion-engineered heterogeneous MCFs for compact fiber-distributed signal processing, i.e., the simultaneous processing and distribution of microwave and optical signals [9]. This approach is based on the custom design of MCFs to act as tunable sampled

#468436 https://doi.org/10.1364/OE.468436
Journal © 2022 Received 21 Jun 2022; revised 29 Jul 2022; accepted 11 Aug 2022; published 23 Aug 2022

Optics EXPRESS

TTDLs where every core provides at the output a different time-delayed version of the incoming signal which, in addition, can be continuously tuned by varying the operating optical wavelength. Such a MCF-based TTDL is particularly attractive for next-generation wireless communications systems, such as Beyond 5G, as it brings further flexibility, versatility, capacity and connectivity along with reduced size, weight, and power consumption.

Up to date, the reported MCF-based optical beamforming networks exploit the MCF for mere distribution while the actual TTDL is implemented externally. In [10], optical beamforming for a 4-element antenna was demonstrated on a Si_3N_4 integrated photonic circuit based on a series of optical ring resonators that actuated as the TTDL. Then, this system was followed by a 150-m 4-core homogeneous MCF with the only functionality of providing antenna connectivity. Limited beam-steering from 11.3° to 23° was demonstrated in a 26-GHz radiofrequency (RF) signal. Optical beamforming for a 50-GHz 2-element antenna was demonstrated in [11] by resorting to two external variable optical time delay lines, after which 2 cores of a 2-km 7-core homogeneous MCF were used, again, only for delivery purposes. Following a different rationale, we proposed in [12] to exploit a heterogeneous MCF to provide both tunable TTDL operation for optical beamforming and short-reach distribution to the antenna. In that work, we simulated the equivalent array factor that could be obtained at 10 GHz from the measured RF phase difference after MCF propagation, but no real antenna beamforming was demonstrated.

In this work, we report, for the first time to our knowledge, the experimental demonstration of optical beamforming for PAAs implemented on a 5-km heterogeneous MCF composed of 7 customized dispersion-engineered cores that offer tunable TTDL operation. We successfully demonstrate radio beam-steering within an 83° range in an in-house fabricated 8-element PAA at the RF frequency of 26 GHz exploiting the dispersion diversity of the MCF.

2. Multicore fiber true-time delay line

We have developed a 7-core heterogeneous MCF that operates as a tunable sampled true time delay line [12,13]. Each fiber core n was designed and fabricated with distinct radial dimensions and core material composition to provide a particular group-delay dependence with the optical wavelength, $\tau_n(\lambda)$. Figure 1(a) shows a photograph of the cross-section of the MCF, which was fabricated by the company YOFC. It is 5-km long and consists of 7 different trench-assisted step-index cores placed in a hexagonal disposition inside a 147.5-μm fiber cladding diameter, with an averaged 41-μm core pitch. The measured worst-case crosstalk for the whole fan-in + MCF + fan-out structure is below -30 dB. The insertion losses range from 4.6 to 7.7 dB, in which the propagation losses measured by an Optical Time Domain Reflectometer at an optical wavelength of 1550 nm are 0.46, 0.31, 0.31, 0.50, 0.19, 0.20, 0.17 dB/km, respectively, for cores 1 to 7.

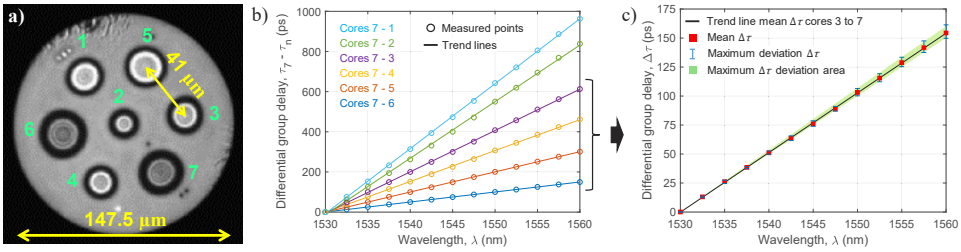

Fig. 1. (a) Photograph of the fabricated MCF cross-section, (b) measured differential group delays with respect to core 7 ($\tau_7 - \tau_n$), and (c) mean value of measured basic differential group delay ($\Delta\tau$) for cores 3 to 7 (red-filled squares), along with the maximum deviation (error bars), the trend line for the mean $\Delta\tau$ (black line) and its estimated maximum deviation area (green area).

Optics EXPRESS

The uniqueness of this fiber lies in the capability of providing the range of chromatic dispersions required for continuously tunable sampled TTDL operation in a single optical fiber. If we exploit the spatial diversity, i.e., each core provides a TTDL sample, at the output of the L-km MCF link we will get a basic differential group delay between adjacent cores ($\Delta\tau = \tau_n$ - τ_{n-1}) that is provided by the differential chromatic dispersion ($\Delta D = D_n$ - D_{n-1}) following $\Delta\tau = \Delta D\lambda L$. Therefore, linearly incremental differential group delays with the optical wavelength require as well linearly incremental chromatic dispersions (i.e., group delay slopes).

Figure 1(b) depicts the measured spectral differential group delays between core 7 and the rest ($\tau_7 - \tau_n$), where we can appreciate, on one hand, how the differential group delay slopes increase linearly with the optical wavelength and, on the other hand, a similar increment from core to core. Actually, the average measured chromatic dispersions D_n at the anchor wavelength $\lambda = 1530$ nm follow that incremental trend with values of 13.85, 14.95, 16.35, 17.30, 18.25, 19.30 and 20.30 ps/(km·nm), respectively for cores 1 up to 7. Cores 3 to 7 provide differential chromatic dispersions ΔD nearly 1 ps/(km·nm), providing a constant basic differential group delay between adjacent samples for optical wavelengths ranging from 1530 up to 1560 nm. However, cores 1 and 2 seem to have been more affected by fabrication inaccuracies and therefore do not provide the required ΔD within a 10-% margin of tolerance. Figure 1(c) illustrates the measured spectral basic differential group delay $\Delta\tau$ for cores 3 to 7. Red-filled squares represent the mean measured differential group delays, error bars show their maximum deviation, and the black solid line represents the trend line for the mean values. We see that these 5 cores provide a linearly incremental basic differential group delay with the optical wavelength without significant deviation in a 30-nm optical wavelength range. Then, up to 5-sample TTDL operation can be implemented in the space-diversity domain by using cores 3 up to 7, while all 7 cores are applicable to operate in the wavelength diversity domain or to implement any other application that does not require space-diversity signal processing with a constant basic differential delay.

3. Phased array antenna

An 8-element microstrip PAA with an element spacing of $d = 5.77$ mm ($0.5\lambda_0$ at 26 GHz) was designed and fabricated. Because of the large electrical size of available RF connectors at this band, an extension of the input lines ending at a stepped substrate outline was conceived to accommodate the connectors. Microstrip lines were properly shaped to ensure identical time delays from each input to its corresponding radiating element. Figure 2(a) shows a 3D representation of the radiation pattern at 26 GHz over the PAA, simulated by CST Microwave Studio, when all inputs are fed with a uniform amplitude and phase. As expected, a directive radiation pattern along array axis is achieved, with a small ripple due to the finite dielectric.

The antenna was fabricated at our facilities using a milling machine on a substrate Rogers RT5880 with a height of 0.381 mm and relative permittivity of 2.2. Figure 2(b) shows a picture of the fabricated antenna, which has been measured in the band of interest. Figure 2(c) represents the active S-parameters as a function of the RF frequency measured with a Vector Network Analyzer (VNA). It can be observed that signal reflection keeps mostly below the accepted threshold of -10 dB within the measured band. Finally, far-field radiation patterns have been measured in an anechoic chamber at 26 GHz. Figure 2(d) compares the measured embedded radiation pattern of one representative antenna element with the simulated one, where the typical rippled response along the non-directive plane is observed, with a -6-dB beamwidth of around 120°.

Optics EXPRESS

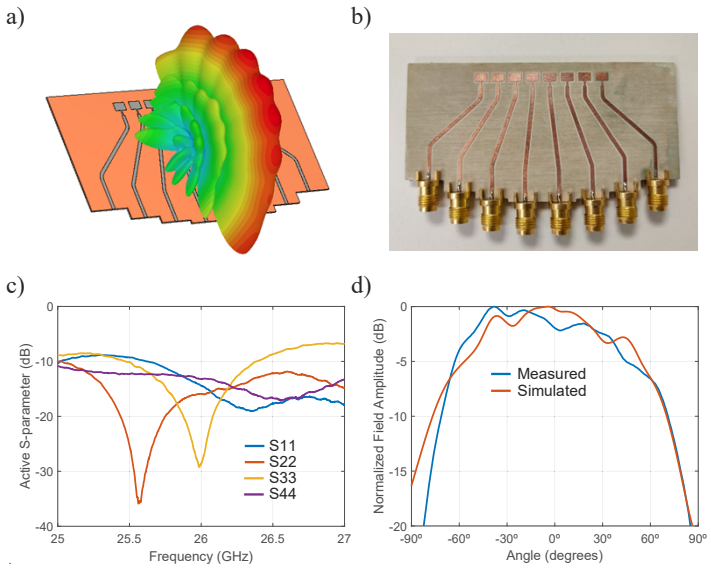

Fig. 2. Phased array antenna. (a) 3D representation of the radiation pattern, (b) photograph of the PAA with the RF connectors, (c) measured active *S*-parameters as a function of the radiofrequency, and (d) measured radiation pattern for a single antenna element compared with the simulated one.

4. Optical beamforming experimental results

We apply the developed MCF-based TTDL to experimentally demonstrate optical beamforming for the PAA at the RF frequency of 26 GHz. By using cores 3 up to 7, we implement a 5-element beamforming network for the PAA whose beam-pointing angle is tuned as we vary the basic differential delay $\Delta\tau$ by changing the laser optical wavelength of operation, as Fig. 1(c) shows.

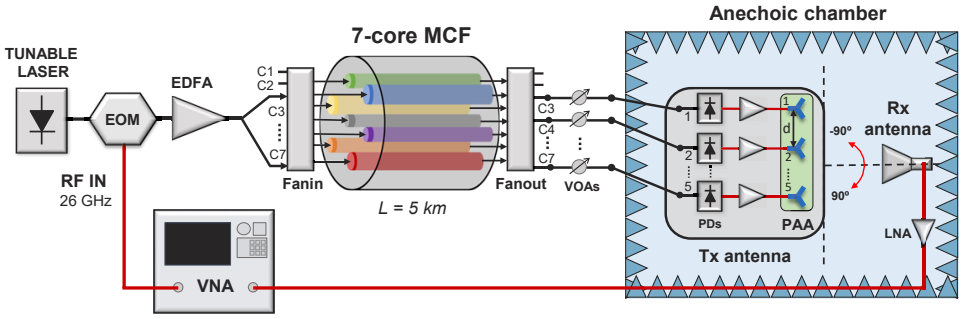

Fig. 3. Experimental setup of the optical beamforming network for the fabricated PAA along with the radiation pattern measurement infrastructure. EOM: Electro-Optic Modulator, EDFA: Erbium-Doped Fiber Amplifier, VNA: Vectorial Network Analyzer, VOA: Variable Optical Attenuator, PD: Photodetector, PAA: Phased Array Antenna, LNA: Low-Noise Amplifier.

Figure 3 represents the experimental setup used to measure the radiation pattern of the PAA in an isolated environment. Here, the optical signal coming from a tunable laser is modulated using a dual-drive external modulator (EOM) with the RF signal generated by a VNA. This signal is then amplified using an erbium doped fiber amplifier (EDFA) and launched into the corresponding

Optics EXPRESS

cores of the 5-km MCF. Variable optical attenuators (VOAs) are placed in each core path to ensure uniform power distribution. The signal from each core is detected and amplified using independent photodiodes and RF amplifiers. The PAA along with the required optical and electrical devices are placed inside the anechoic chamber and onto an antenna positioner. The received power is then measured by means of a receiver horn antenna and amplified by a low noise amplifier (LNA) to obtain the radiation pattern with the help of the VNA.

Figure 4 shows the inside of the anechoic chamber, where we can appreciate in the left photograph the front side of the transmitter antenna and in the right photograph the receiver antenna. The separation between both antennas is 3 meters. The transmitter antenna is held in an antenna positioner that allows a 180-degree azimuth rotation for the proper measurement of the radiation pattern. The MCF spool is placed outside the anechoic chamber. As we can see in the left photograph, after the fan-out, each output fiber is connected to an independent photodetector and RF amplifier, which are placed on the antenna positioner, and feeds the corresponding PAA input by means of a 1-meter RF cable.

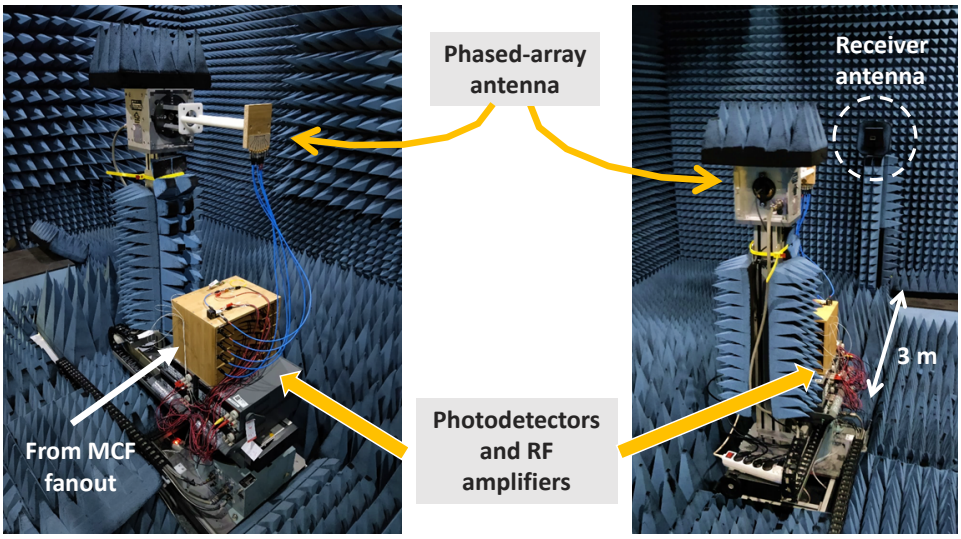

Fig. 4. Photographs of the inside of the anechoic chamber with identification of both antennas along with main devices at the transmitter side.

Beam steering in the optical beamforming network is achieved by sweeping the operation optical wavelength. Figure 5(a) illustrates the evolution of the beam pointing angle as a function of the optical wavelength. Different optical wavelength bands can be chosen to produce a beam steering of 180° in the typical EDFA optical wavelength range (i.e., 1530–1560 nm). As the single element radiation pattern of Fig. 2(d) shows, for absolute angles greater than 45°, the received power drops considerably, what limits the maximum beamforming angle we can achieve. Thus, we choose the optical wavelength band ranging from 1542.50 up to 1548.28 nm, which produces the desired range of beam pointing angles.

We then measured the radiation pattern at different optical wavelengths ranging from 1542.50 to 1548.28 nm in steps of 0.96 nm. This translates into time delays provided by the TTDL going from 62.5 to 91.36 ps in steps of 4.81 ps approximately. Figure 5(b) depicts the measured radiation pattern for the 7 different optical wavelengths. The resulting beam pointing angle varies approximately from -43° up to 40°. Minor discrepancies on the basic differential delay between cores affect the radiation pattern, causing main lobe broadening at angles farther from broadside direction and shifting the beam pointing angle slightly. The radiation pattern of the antenna

Optics EXPRESS

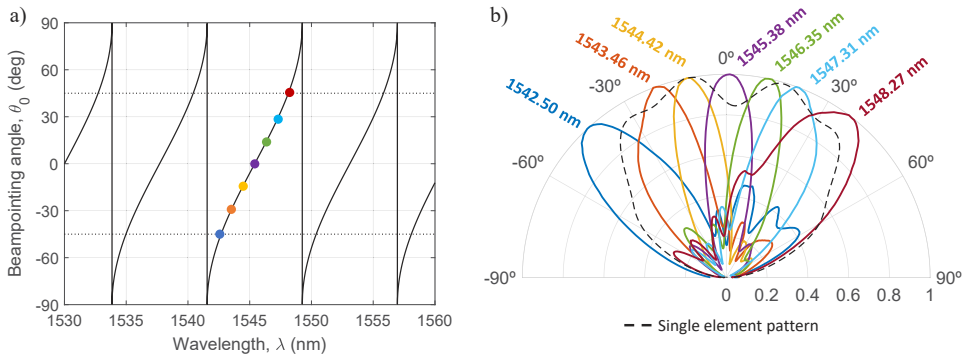

Fig. 5. (a) Simulation of the beam-pointing angle (in degrees) as a function of the optical wavelength. Filled circles indicate the chosen wavelengths for the experiment. (b) Measured radiation patterns of the whole PAA at different wavelengths (colored solid lines) together with that of a single radiating element of the PAA (black dashed line).

elements also takes part here as it has substantial power variations, affecting the main lobe shape. In addition, slight mismatches between the theoretical and experimental beam pointing direction for angles farther than broadside can also be attributed to the antenna itself due to the higher attenuation for those angles, as the single element radiation pattern shows (black dashed line in Fig. 5(b)).

We must note that high levels of intercore crosstalk could contribute to the main lobe broadening and reduce the main-to-side-lobe ratio. However, in our case, crosstalk among the five cores exploited for optical beamforming remains below -40 dB, resulting in no significant effect on the radiation pattern.

5. Discussion

The performance of the implemented optical beamforming network could be affected by static sources of degradation, such as fiber bending and twisting, as well as by dynamic environmental fluctuations caused mainly by temperature deviations. Since once the MCF link is deployed in a given scenario, one should not expect significant fiber bending and twisting (which can be compensated once the system is set up), we will focus on possible temperature fluctuations. In [13], we experimentally evaluated the influence of temperature on the differential group delay between cores in a temperature-controlled chamber, observing a maximum skew below 1 ps/°C. From that measurement, we draw in Fig. 6 the effect on the RF phase shift difference between adjacent cores at 26 GHz from 15 °C to 35 °C, where the maximum difference remains below 60° (i.e., less than 6°/°C). Such a worst-case value would translate into an antenna beam misalignment of 2°/°C, which corresponds to a hypothetical situation where the phase difference between every pair of cores is given by the maximum value of 6°/°C. As we can see from the different curves in Fig. 6, such a scenario is very unlikely.

All in all, our radio beam-steering experiment was carried in a controlled environment (anechoic chamber) where the temperature variation was kept below 1°C. In that case, the beam misalignment remains below 1°. Depending on the application scenario, if considerable temperature fluctuations are expected, then some type of dynamic optimization of the differential time delay should be implemented after propagation through the MCF.

Beyond the 1D-beamforming experiment successfully demonstrated in this paper, dispersion-diversity MCF TTDLs have the potential to enable reconfigurable 2D-beamforming by exploiting not only the dispersion-diversity dimension provided by the MCF, but also the wavelength-diversity dimension if we inject a set of equally-spaced optical wavelengths. While dispersion

Optics EXPRESS

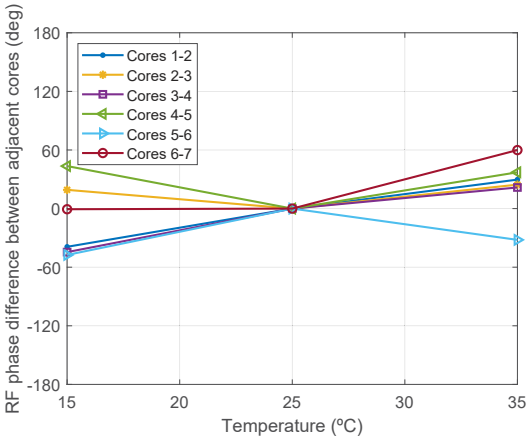

Fig. 6. Temperature dependence of the RF phase shift difference between adjacent cores.

diversity allows for azimuth beam-steering by using the wavelength dependence of the core differential delays ($\Delta\tau = \Delta D\lambda L$), wavelength diversity will introduce elevation beam-steering by exploiting each core dependence of the differential delay between adjacent wavelengths ($\Delta\tau = D_n\delta\lambda L$ in core n, where $\delta\lambda$ is the separation between adjacent wavelengths). We must note that the addition of wavelength diversity will increase complexity and cost, as compared to the solely use of space diversity, because a multicarrier optical source, a wavelength multiplexer, and a series of wavelength demultiplexers will be needed, (similarly to other dispersive-fiber-based approaches exploiting wavelength diversity, as for instance [3] and [4]).

6. Conclusions

We have experimentally demonstrated, for the first time to our knowledge, continuously tunable optical beamforming for phased array antennas built upon a custom dispersion-engineered heterogeneous multicore fiber. The 5-km fiber comprises 7 different trench-assisted cores, where the refractive index profile of each core was individually addressed to fulfil the requirements for tunable sampled TTDL operation while providing low intercore crosstalk. Continuous beam-steering was demonstrated by measuring the radiating pattern of an in-house 8-element phased array antenna in an anechoic chamber at the RF frequency of 26 GHz, sweeping the beam-pointing angle from -43° up to 40° by varying the operating optical wavelength from 1542.50 up to 1548.28 nm.

All in all, dispersion-diversity MCFs open the door towards the implementation of compact and versatile fiber-distributed signal processing, where both distribution and processing functionalities are provided within the same fiber medium. Other RF and optical signal processing functionalities, such as tunable microwave signal filtering, arbitrary waveform generation as well as time differentiators or integrators, can also be implemented by this approach.

Funding. Ministerio de Ciencia e Innovación (PID2020-118310RB-100); Universitat Politècnica de València (PAID-10-21); Generalitat Valenciana (IDIFEDER/2020/032); European Research Council (724663).

Disclosures. The authors declare no conflicts of interest.

Data availability. Data underlying the results presented in this paper are not publicly available at this time but may be obtained from the authors upon reasonable request.

References

1. I. Frigyes and A. Seeds, "Optically generated true-time delay in phased-array antennas," IEEE Trans. Microwave Theory Tech. **43**(9), 2378–2386 (1995).

Optics EXPRESS

2. R. D. Esman, M.Y. Frankel, J.L. Dexter, L. Goldberg, M.G. Parent, D. Stilwell, and D.G. Cooper, "Fiber-optic prism true time-delay antenna feed," IEEE Photonics Technol. Lett. **5**(11), 1347–1349 (1993).
3. K. Ito, M. Suga, Y. Shirato, N. Kita, and T. Onizawa, "Remote beamforming scheme with fixed wavelength allocation for radio-over-fiber systems employing single-mode fiber," J. Lightwave Technol. **40**(4), 997–1006 (2022).
4. B. Jung and J. Yao, "A two-dimensional optical true time-delay beamformer consisting of a fiber bragg grating prism and switch-based fiber-optic delay lines," IEEE Photonics Technol. Lett. **21**(10), 627–629 (2009).
5. S. R. Forrest and R. B. Taylor, "Optically controlled phased array radar," in *1996 International Topical Meeting on Microwave Photonics (MWP '96)*, Kyoto, Japan (1996), 193–196.
6. M. Burla, D. Marpaung, L. Zhuang, A. Leinse, M. Hoekman, R. Heideman, and C. Roeloffzen, "Integrated photonic Ku-band beamformer chip with continuous amplitude and delay control," IEEE Photonics Technol. Lett. **25**(12), 1145–1148 (2013).
7. A. Tikhomirov, E. Omelyanchuk, and A. Semenova, "Recommended 5G frequency bands evaluation," in *Systems of Signals Generating and Processing in the Field of on Board Communications*, Moscow, Russian Federation (2018), 1–5.
8. D. J. Richardson, J. M. Fini, and L. E. Nelson, "Space-division multiplexing in optical fibres," Nat. Photonics **7**(5), 354–362 (2013).
9. S. García and I. Gasulla, "Dispersion-engineered multicore fibers for distributed radiofrequency signal processing," Opt. Express **24**(18), 20641–20654 (2016).
10. M. Morant, A. Trinidad, E. Tangdiongga, T. Koonen, and R. Llorente, "Experimental Demonstration of mm-Wave 5G NR Photonic Beamforming Based on ORRs and Multicore Fiber," IEEE Trans. Microwave Theory Tech. **67**(7), 2928–2935 (2019).
11. A. Morales, I. T. Monroy, F. Nordwall, and T. Sørensen, "50 GHz optical true time delay beamforming in hybrid optical/mm-wave access networks with multi-core optical fiber distribution," Chin. Opt. Lett. **16**(4), 040603 (2018).
12. S. García, M. Ureña, and I. Gasulla, "Heterogeneous multicore fiber for optical beamforming," in *2019 International Topical Meeting on Microwave Photonics (MWP2019), Ottawa, Canada* (2019).
13. S. García, M. Ureña, and I. Gasulla, "Dispersion-diversity multicore fiber signal processing," ACS Photonics **9**(8), 2850–2859 (2022).